Two-dimensional electron gas at the AlGaN/GaN interface

Layer thickness dependence

Popok, Vladimir; Caban, Piotr; Michalowski, Pawel Piotr; Thorpe, Ryan; Feldman, Leonard; Pedersen, Kjeld

Published in:
Journal of Applied Physics

DOI (link to publication from Publisher):
10.1063/1.5142766

Publication date:
2020

Document Version
Publisher's PDF, also known as Version of record

Journal of Applied Physics

Two-dimensional electron gas at the AlGaN/GaN interface: Layer thickness dependence

Cite as: J. Appl. Phys. **127**, 115703 (2020); https://doi.org/10.1063/1.5142766
Submitted: 17 December 2019 . Accepted: 04 March 2020 . Published Online: 18 March 2020

Vladimir N. Popok, Piotr A. Caban, Pawel Piotr Michalowski, Ryan Thorpe, Leonard C. Feldman, and Kjeld Pedersen

Journal of Applied Physics ARTICLE scitation.org/journal/jap

Two-dimensional electron gas at the AlGaN/GaN interface: Layer thickness dependence

Cite as: J. Appl. Phys. **127**, 115703 (2020); doi: 10.1063/1.5142766
Submitted: 17 December 2019 · Accepted: 4 March 2020 ·
Published Online: 18 March 2020

Vladimir N. Popok,[1,a)] Piotr A. Caban,[2] Pawel Piotr Michalowski,[2] Ryan Thorpe,[3] Leonard C. Feldman,[3] and Kjeld Pedersen[1]

AFFILIATIONS

[1]Department of Materials and Production, Aalborg University, 9220 Aalborg, Denmark
[2]Institute of Electronic Materials Technology, 01-919 Warsaw, Poland
[3]Department of Physics & Astronomy, Rutgers, The State University of New Jersey, Piscataway, New Jersey 08854, USA

[a)]**Author to whom correspondence should be addressed:** vp@mp.aau.dk

ABSTRACT

In the current paper, the structure and properties of AlGaN/GaN interfaces are studied, explaining the role of AlGaN layer thickness on the two-dimensional electron gas (2DEG) formation. It is found that the generation of a continuous electron gas requires AlGaN films with stable stoichiometry, which can be reached only above a certain critical thickness, ≈6–7 nm in our case (20 at. % Al content). Thinner films are significantly affected by oxidation, which causes composition variations and structural imperfections leading to an inhomogeneity of the polarization field and, as a consequence, of the electron density across the interface. Using Kelvin probe force microscopy, this inhomogeneity can be visualized as variations of the surface potential on the sub-micrometer scale. For heterostructures with layer thickness above the critical value, the surface potential maps become homogeneous, reflecting a weakening influence of the oxidation on the interface electronic properties. The 2DEG formation is confirmed by the Hall measurements for these heterostructures.

I. INTRODUCTION

The wide bandgap semiconductor GaN provides attractive properties such as high breakdown field, high thermal conductivity, and high charge carrier velocity, making it of great interest for power switching devices.[1,2] An additional desirable aspect is the formation of a two-dimensional electron gas (2DEG) at the interface with another III-N semiconductor, typically AlGaN, enabling the fabrication of high electron mobility transistors.[3–6] In the last decade, such heterostructures, possessing 2DEG, were also in high demand for applications in THz electronics.[7,8]

At the epitaxially grown AlGaN/GaN interface, the lattice mismatch and difference in coefficients of thermal expansion (CTE) lead to strain formation. Since nitride semiconductors lack a center of inversion symmetry, the presence of strain causes piezoelectric polarization. Additionally, there is a spontaneous polarization due to the difference in electronegativity of these III-N materials. In the case of a Ga-faced GaN buffer with top AlGaN layer, the total polarization causes a positive net charge on the AlGaN side, requiring "negative" compensation from GaN in the form of 2DEG,[9] which is associated with the donor-like surface states.[10]

For device fabrication, GaN is typically grown as a micrometer thick film on substrates of sapphire, silicon, or silicon carbide. Due to the lattice and CTE mismatches, the synthesized GaN films suffer from a high concentration of threading dislocations (TDs), which also affects the crystalline quality of the epitaxial AlGaN layer grown on the top and properties of the 2DEG at the interface.[11–14] In addition to crystallinity, one needs to consider the composition (Al content x, $Al_xGa_{1-x}N$) and layer thickness. Both parameters are found to affect the charge carrier concentration and mobility.[4,15] An increase in x, on the one hand, facilitates higher electron concentration due to stronger polarization fields at the interface but, on the other hand, increases the lattice mismatch causing higher strain, impairing the electron mobility. To reach a compromise, Al content is suggested to be optimal in the 20%–30% range.[16–18] There are also several practical reasons to control AlGaN thickness, which affects the gate leakage current, Schottky barrier at metal electric contacts, and 2DEG parameters.[19–21] It was found that a critical (minimal) thickness of the AlGaN layer is required in order to initiate the 2DEG. The further thickness increase affects both the electron density and mobility but with opposite tendencies: the

former increases while the latter decreases with the thickness.[15] These tendencies again require a compromise yielding a rather narrow thickness interval, typically between 15 and 30 nm.[16–18,21] Nevertheless, the issue of critical thickness is rather poorly studied. The available publications about the critical thickness of AlGaN report that a layer of 4–6 nm is needed in order to enable 2DEG formation.[10,22] A correlated finding was reported in Ref. 23, where no 2DEG formation was observed for the $Al_{0.25}Ga_{0.75}N$ layer with a thickness of 3 nm. To our knowledge, there are no models explaining the physical reasons for the critical thickness and no reports on the dynamics of 2DEG formation under a thickness transition from below to above a critical value.

In the current paper, we present the results on studies of thin (from ca. 2 to 12 nm) layers of AlGaN grown on GaN in order to evaluate critical thickness for 2DEG nucleation and bring new insights into dynamics of the electron gas formation.

II. SAMPLE GROWTH AND EXPERIMENTAL METHODS

AlGaN/GaN heterostructures were grown on 2-in. single side polished (0001)-oriented sapphire substrates with a maximum miscut angle of 0.2° to the m-plane. The synthesis was performed using an AIX 200/4 RF-S metal-organic chemical vapor deposition low-pressure reactor utilizing source gases of trimethylaluminum, trimethylgallium, and ammonia, and hydrogen as the carrier gas. The reactor parameters (pressure, temperature, and gas fluxes) for all III-N fabricated layers were very similar to those described in Ref. 11. Growth was carried out by the formation of a thin AlN nucleation (low temperature) layer; further growth at higher temperature yielding in total 745 ± 15 nm thick AlN films; and a 1090 ± 150 nm thick GaN buffer synthesis. These thicknesses were established via cross-sectional scanning electron microscopy. One of the GaN wafers is used as a reference sample while layers of increasing thickness of AlGaN are fabricated on another six wafers (samples 1–6) keeping the same synthesis parameters except the growth time of the top layer.

Evaluation of the composition and the thickness of these nanometer thin layers was carried out by secondary ion mass spectroscopy (SIMS), x-ray photoelectron spectroscopy (XPS) assisted by sputtering, and transmission electron microscopy (TEM). SIMS measurements were performed employing the CAMECA SC Ultra instrument under ultrahigh vacuum conditions of 4×10^{-10} mbar. Sufficient depth resolution was obtained for negative ion detection mode using a Cs^+ primary beam with an energy of 150 eV allowing to analyze $200 \times 200\,\mu m^2$ areas. TEM measurements were carried out using the Philips EM420 microscope at an accelerating voltage of 100 kV. For x-ray photoelectron spectroscopy (XPS) measurements, a Thermo Scientific K-Alpha spectrometer was utilized. The x-ray beam was produced by a monochromated Al Kα source with an energy of 1486.6 eV. The total instrumental resolution was 0.5 eV. In order to avoid charging during the measurements, a low energy dual beam Ar^+ and electron flood gun was directed at the sample. The binding energy of the peaks was calibrated using the main component of the adventitious carbon peak at 284.8 eV. In order to determine the composition of the films as a function of depth, ion beam etching was performed in 10 s increments using 1 keV Ar^+ ions, which removed about 0.3 nm of AlGaN per cycle. Hall and Kelvin probe force microscopy (KPFM) measurements were used to determine the properties of the 2DEG. Electrical parameters were obtained using the van der Pauw method. The AlGaN/GaN heterostructures were prepared in square shapes (7×7 mm^2) with contacts made of pure indium 6*N* and placed in the corners. Measurements were carried out in a magnetic field of 1 T at room (300 K) and liquid nitrogen (77 K) temperatures using a system composed of Keithley units (model 7065 card, DC power supply model 6221, nanovoltmeter model 2182) and triaxial cables, which together provided a very high input resistance ($10^{12}\,\Omega$) and high accuracy in voltages measurements. The KPFM was performed

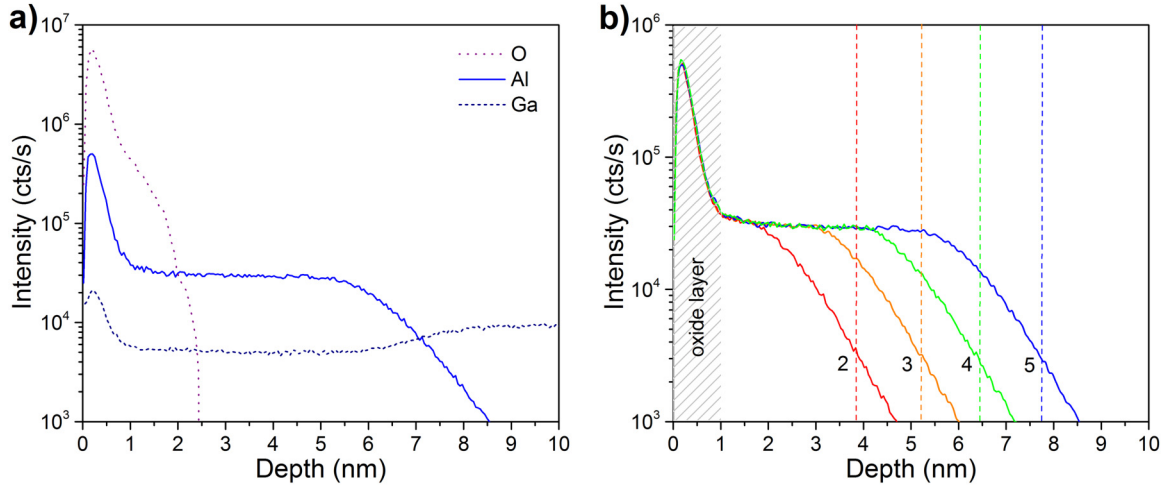

FIG. 1. SIMS depth profiles (a) of oxygen, aluminum, and gallium in sample 5 and (b) of aluminum in samples 2–5 corresponding to increasing thickness of the AlGaN layer. Dashed vertical lines in panel (b) show the concentration cutoff corresponding to decrease for one order of magnitude.

TABLE I. Al concentration calculated from XPS data and thickness of AlGaN films found by different methods indicated in parentheses.

Sample No.	Al (at. %)	Thickness (nm)
1	7	1.6 (XPS)
2	15	3.8 (SIMS), 3.3 (XPS)
3	20	5.2 (SIMS), 4.9 (XPS)
4	20	6.5 (SIMS), 7.3 (XPS)
5	18	7.8 (SIMS)
6	21	12.5 (TEM)

using Ntegra-Aura nanolaboratory and the two-pass technique described in detail elsewhere.[24] Commercial silicon cantilevers with gold conductive coating (tip curvature radius ≤35 nm) were used providing a lateral resolution of KPFM images better than 100 nm.

III. RESULTS AND DISCUSSION

Depth profiles obtained by SIMS [Fig. 1(a)] show the presence of oxygen in a thin surface layer indicative of oxidation of Al and Ga. The intense peaks of Al and Ga within the first nanometer of the layer are artifacts associated with the increased sputtering efficiency and enhanced charge states due to the presence of an oxide. Similar surface peaks of Al and Ga are found on all studied samples. For this reason, it became impossible to obtain a reliable depth profile for sample 1 with the thinnest AlGaN layer. For samples 2–5, the Al and Ga profiles become constant at a higher depth indicating the formation of AlGaN films with stable stoichiometry. Thereafter, the Al concentration decreases while Ga concentration rises to the next constant value indicating the transition to pure GaN. This transition occurs on the length scale of about 2 nm. Thus, monitoring the Al profiles [see Fig. 1(b)] allows an estimate of the thicknesses of the top AlGaN layers as presented in Table I. Figure 1(b) also shows that the Al concentration is the same in all grown layers, indicative of a stable AlGaN stoichiometry from sample to sample.

Using XPS, concentrations of Al, Ga, and N are found by evaluation of Al 2p, Ga 3d, and N 1s peaks (see Fig. 2). The Ga 3d spectrum exhibits several sets of doublets, indicating the presence of elemental Ga and oxidized AlGaN as well as stoichiometric AlGaN. The presence of oxide is consistent with the SIMS results. Unfortunately, the peak N 1s cannot be precisely deconvoluted and quantified because of its overlap with the Ga LMM (Auger) peak. This uncertainty in the nitrogen content affects the precision of Al and Ga concentration calculation. The results for Al are presented in Table I yielding the values between 18 and 21 at. % for samples 3–6. Note that the Al percentage measured for samples 1 and 2 is lower due to the contribution of the underlying GaN. The AlGaN layers of these samples are so thin that the photo-exited electrons are also detected from the GaN buffer, thus artificially decreasing the real Al/Ga ratio in AlGaN. However, taking into consideration the SIMS spectra presented in Fig. 1(b), which show the same Al concentration for samples 2–5, we can disregard this artifact and conclude that Al content is the same in all samples, i.e., approximately 20 at. %.

XPS measurements were also carried out in combination with the sputtering of AlGaN films. Figure 3 shows a decrease of Al 2p peak intensity with sputtering time for sample 2. Assuming the same sputtering coefficient for all films in question, the thickness of the Al containing layer can be found. These data are added to Table I showing a reasonable agreement with the values obtained by SIMS for samples 2–4. For samples 5 and 6, ion beam mixing of atoms in the film and bulk made the XPS thickness measurements unreliable, and the film thicknesses were estimated from SIMS and TEM, respectively. The TEM image of sample 6 is shown in Fig. 4.

For heterostructures with AlGaN thickness ≤5 nm (samples 1–3), Hall measurements showed resistance ρ on the MΩ scale,

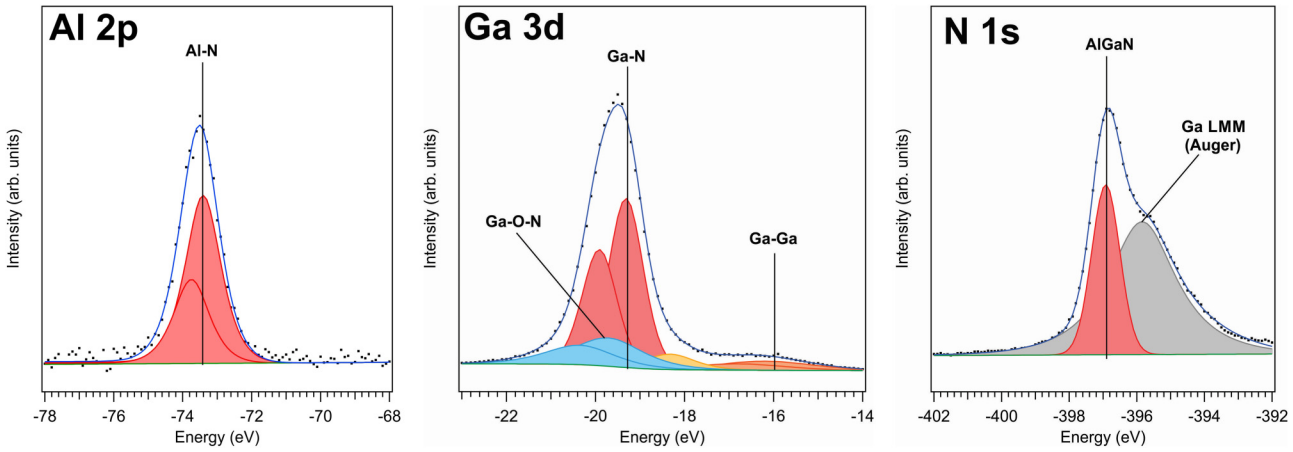

FIG. 2. Measured XPS spectral elements corresponding to Al 2p, Ga 3d, and N 1s (dot curves with blue fits) with corresponding convolution plots for different components highlighted in different colors. Red plots correspond to stoichiometric AlGaN. In Al and Ga panels, two red curves reflect doublets due to the spin–orbit splitting. In the Ga panel, blue plots correspond to oxidized AlGaN/GaN, yellow one to possibly of N deficient AlGaN/GaN, and orange plot to elemental Ga.

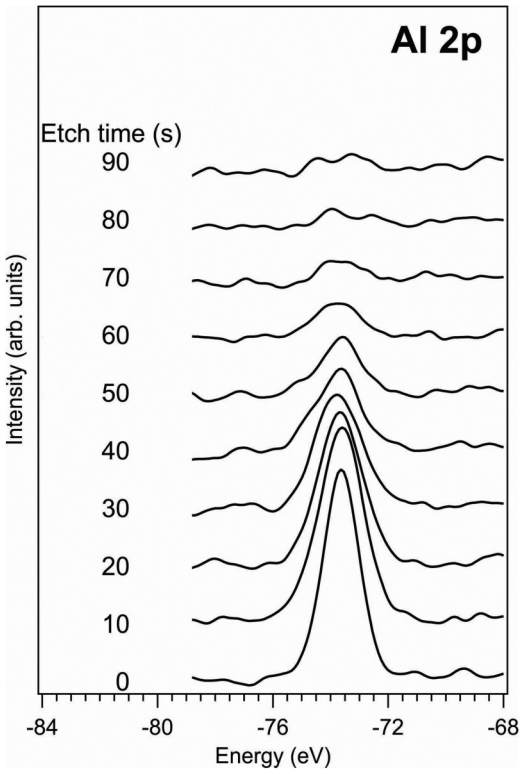

FIG. 3. Intensity decrease of the Al 2p peak with increasing sputtering (etch) time for sample 2.

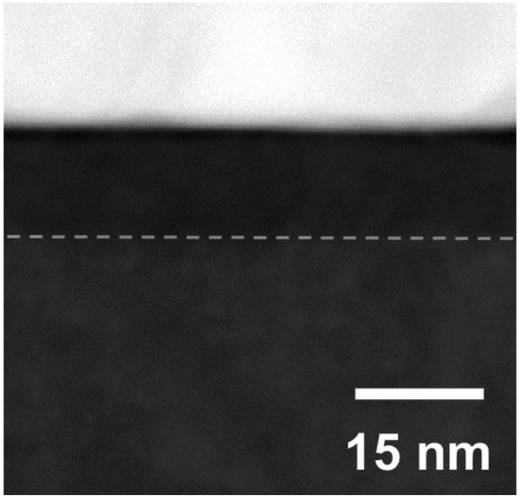

FIG. 4. TEM image of the AlGaN/GaN interface (visualized by the dashed line) for sample 6.

thus yielding very low charge carrier concentration n and electron mobility μ, suggesting that there is no continuous 2DEG formed across the interface. For sample 4 with a ≈7 nm thick AlGaN layer, ρ drops to the kΩ level, yielding $n = 1.35 \times 10^{12}$ cm^{-2} and $\mu = 403.6$ cm^2/V s at room temperature (Table II). Measurements at 77 K show lower resistance and higher carrier concentration and mobility, as expected. Slight increase of AlGaN thickness (sample 5) leads to the increase of both n and μ. For sample 6, with a ≈12 nm thick AlGaN layer, the carrier concentration further increases while the mobility decreases. The decrease is particularly high (more than two times) at low temperature. This tendency is in good agreement with the one found in Ref. 15 indicating that the thicker layer introduces higher stress, thus decreasing the crystalline quality at the interface and increasing scattering of the charge carriers.

Topography of the reference (GaN) sample can be seen in Fig. 5(a). The AFM image shows a typical surface texture with terraces. The height variations across the surface reach approximately 7 nm yielding a root mean square roughness value of 1.3 nm. AlGaN layers epitaxially grown on top of GaN follow its topography (not shown) and have very similar roughness values. TDs formed in GaN are terminated at the surface as small conical shape pits known as V-defects.[11,25,26] In Fig. 5(c), these defects are visible as black dots. The surface density is calculated to be $(2.5 \pm 0.7) \times 10^9$ cm^{-2}. The analyses of sample 1 (with the thinnest AlGaN layer) and 5 (the second thickest layer) both show the value of $\approx 3.0 \times 10^9$ cm^{-2}, which is essentially the same (within the standard deviation) as for the reference sample indicating that the TDs formed in GaN are transferred into the AlGaN epilayers.

KPFM yields the contact potential difference (CPD) between the tip and the surface. For the GaN sample, CPD is measured at different surface positions and the mean value is calculated to be 0.72 ± 0.02 V. Ideally, this value indicates the work function difference of the tip and sample materials. However, the measurements are done in air, and we cannot exclude the presence of a thin liquid layer (due to humidity) on the surface, which can affect the measured CPD. The map of potential variations in Fig. 5(b) shows a very homogeneous distribution across the surface supporting the assumption of homogeneity of the electronic properties (electron density) in a top GaN layer.

KPFM images of the samples with AlGaN films presented in Fig. 6 show distinct changes compared to GaN. The mean CPD values given in Table III are much greater than that of GaN. This is expected as the bandgap of AlGaN is larger than that of GaN while

TABLE II. Contact resistance, charge carrier concentration, and mobility measured by the Hall method at room temperature and 77 K.

Sample	AlGaN thickness (nm)	T (K)	ρ (kΩ/cm^2)	n (10^{12} cm^{-2})	μ (cm^2/V s)
4	≈7	300	11.49	1.35	403.6
		77	0.97	2.65	2422.1
5	≈8	300	3.45	2.36	765.8
		77	0.24	4.05	6298.7
6	≈12	300	2.38	4.56	575.4
		77	0.50	4.40	2862.7

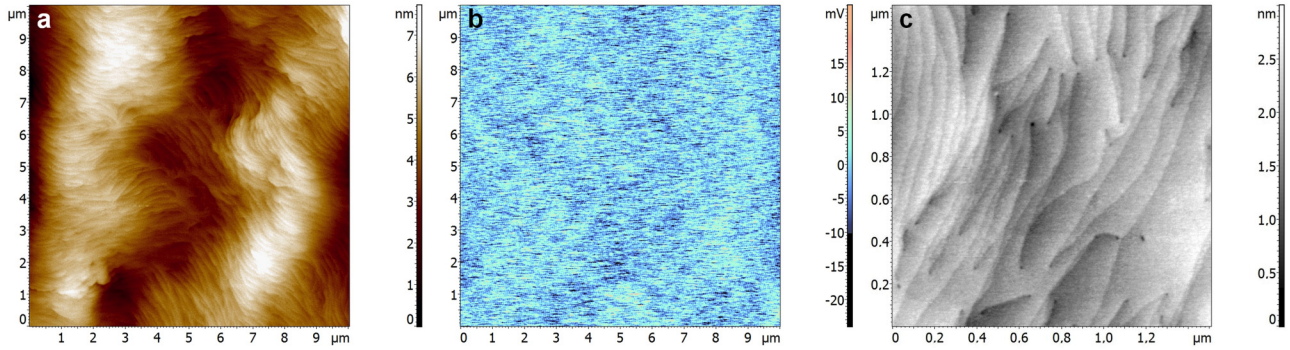

FIG. 5. (a) AFM and (b) KPFM 10 × 10 μm^2 images of the GaN surface (reference sample) as well as (c) AFM image on a smaller scale of 1.5 × 1.5 μm^2 visualizing V-defects (black dots).

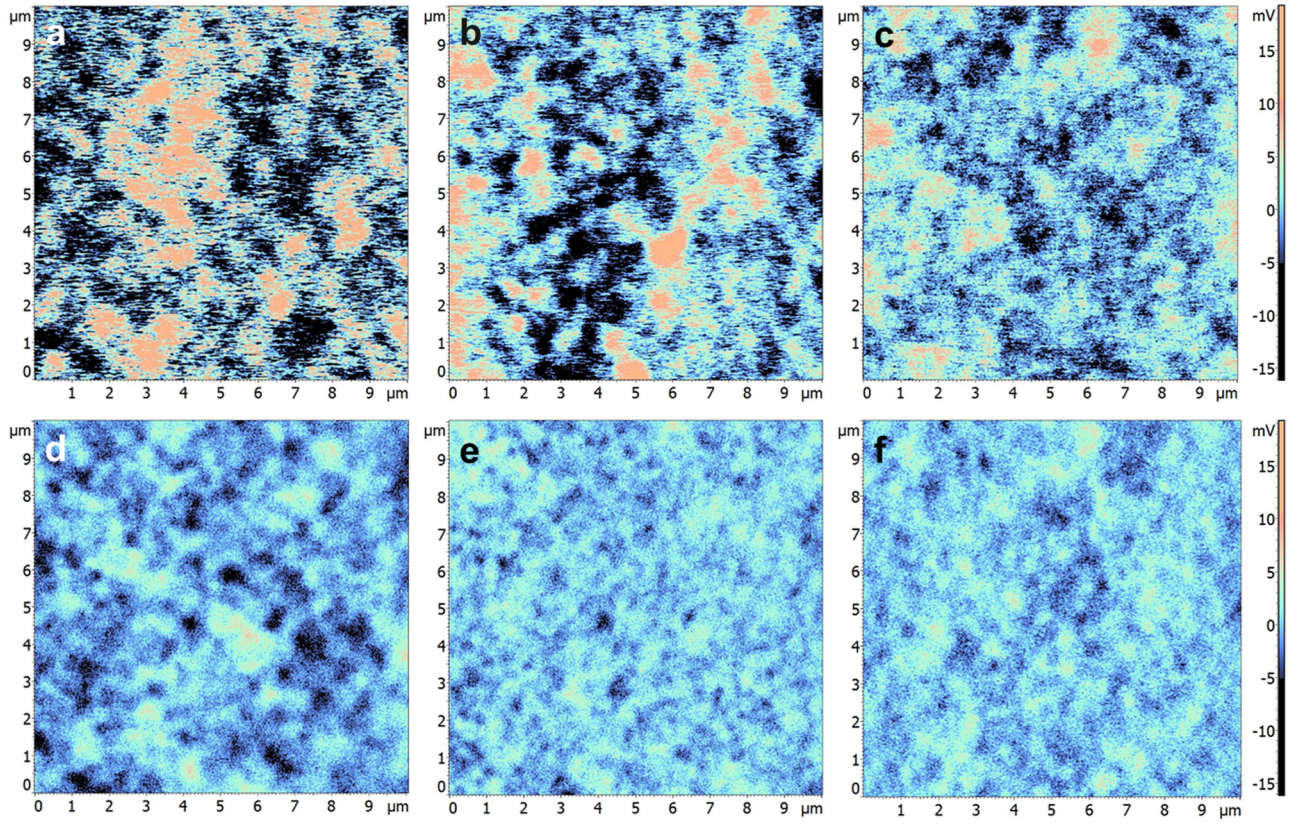

FIG. 6. KPFM images of samples 1–6 with increasing AlGaN layer thickness: (a) ≈1.5 nm, (b) ≈3.5 nm, (c) ≈5 nm, (d) ≈7 nm, (e) ≈8 nm, and (f) ≈12 nm.

TABLE III. Measured CPD values for samples 1–6.

Sample	1	2	3	4	5	6
CPD, V	1.26 ± 0.05	1.24 ± 0.03	1.23 ± 0.03	1.20 ± 0.02	1.25 ± 0.01	1.22 ± 0.01

the electron affinity is smaller, ca. 2.5 eV for $Al_{0.2}Ga_{0.8}N$ compared to 3.3 eV for GaN.[27] This implies a larger difference between the work function of the tip (Au in both case) and $Al_{0.2}Ga_{0.8}N$ compared to GaN. The images for samples 1–3 [panels (a)–(c) of Fig. 6] show highly inhomogeneous, "mosaic-like" potential distributions across the studied areas. The deviations for the mean CPD value (see Table III) are also high. The observed inhomogeneity reflects variations of electronic properties of the AlGaN layer and interface with GaN. Reasons for these variations can be local fluctuations of Al concentration and surface reconstruction caused by the oxide layer formation,[28] which is found by SIMS in our case. These effects should be especially pronounced for the thinner layers. For example, in sample 2, the AlGaN layer thickness is around 3.5 nm, which is equivalent to seven unit cells (lattice parameter c is 0.5185 nm for GaN and 0.4980 nm for AlN in the wurtzite structure). Oxygen is found to the depth of 1.0 nm [Fig. 1(b)]. Thus, at least two unit cells of AlGaN in thickness should be corrupted by oxygen. Similar, but less pronounced effects can be expected for sample 3, with thickness equivalent to ten unit cells, while it should be a very large effect for sample 1 with the layer thickness equivalent of only three unit cells.

Variations of Al concentration cause alterations of spontaneous polarization, while the reconstruction of the crystalline structure affects piezoelectric polarization. Local changes of the polarization field influence the interface net charge and electron density; thus, they can be the origin of the "mosaic-like" maps of surface potential [Figs. 6(a)–6(c)]. In Hall measurements, we found very high resistivity for these samples. Thus, we can conclude that there is no continuous electron gas formed at the interface if the AlGaN layer is below a critical thickness. Increasing the layer thickness (samples 4–6) reveals a transition to more homogeneous surface potential maps [see Figs. 6(d)–6(f)]. For these samples, the surface phenomena (oxidation, Al concentration variations, crystalline imperfections) affect the homogeneity of polarization field at the interface to a lesser extent facilitating the formation of quasi-continuous or continuous 2DEG, which is consistent with the Hall measurements (see Table II). Hence, it can be concluded that a transition from "mosaic-like" to homogeneous KPFM images correlates well with the formation of 2DEG. Based on the obtained results, we suggest a critical thickness of the AlGaN layer for the 2DEG formation to be approximately 6–7 nm for 20 at. % of Al.

It is worth mentioning that a similar evolution from an island-like to homogeneous surface potential distribution was found by KPFM for $LaAlO_3/SrTiO_3$ heterostructures,[24] which are also known for 2DEG generation at the interface. Studies[29] revealed that the Al concentration in the surface layers of $LaAlO_3$ with a thickness below the critical value is not stable across the surface, and the surface potential inhomogeneity observed by KPFM reflects these variations of composition through the local alterations of electron density. Transition to the stable stoichiometry, occurring above the certain critical thickness of the $LaAlO_3$, was found to be in good agreement with the evolution toward homogeneous surface potential maps and was attributed to quasi-continuous 2DEG generation. Similar to our case, the presence of extrinsic defects in the $LaAlO_3$ film was found to be the main reason significantly affecting the interface conductivity.[30]

IV. CONCLUSION

The 2DEG at the interface between the AlGaN layer and GaN buffer is studied, and a physical model explaining the role of the layer thickness on the electron gas formation is suggested. It is found that the AlGaN layers thinner than approximately 6–7 nm are significantly affected by the surface oxidation, which causes variations in composition and crystalline structure and, hence, lead to the strong inhomogeneity of the polarization field at the interface. This inhomogeneity affects the density of electrons attracted to the interface and can be visualized as variations of the surface potential on the sub-micrometer scale in the KPFM images. With increasing layer thickness, the measured surface potential maps become more homogeneous, reflecting the effects of weakening of surface oxidation and reconstruction on the interface electronic properties. Above a critical thickness, which is found for our heterostructures (20 at. % of Al) to be ≈6–7 nm, KPFM represents a relatively homogeneous potential distribution across the surface, and Hall measurements show the electrical parameters (carrier concentration and mobility) consistent with 2DEG formation.

ACKNOWLEDGMENTS

The authors would like to thank Dr. Søren Nielsen from the Aarhus University for help with TEM measurements. They also acknowledge the financial support from the Innovation Fund Denmark under the project "Semiconductor materials for power electronics—SEMPEL."

REFERENCES

[1]J. Millan, P. Godignon, X. Perpina, A. Perez-Tomas, and J. Rebollo, IEEE Trans. Power Electron. **29**, 2155 (2014).
[2]A. Christou and D. Shahin, ECS Trans. **64**, 203 (2014).
[3]E. T. Yu, G. J. Sullivan, P. M. Asbeck, C. D. Wang, D. Qiao, and S. S. Lau, Appl. Phys. Lett. **71**, 2794 (1997).
[4]O. Ambacher, J. Smart, J. R. Shealy, N. G. Weimann, K. Chu, M. Murphy, W. J. Schaff, L. F. Eastman, R. Dimitrov, L. Wittmer, M. Stutzmann, W. Rieger, and J. Hilsenbeck, J. Appl. Phys. **85**, 3222 (1999).
[5]F. Zeng, J. Xilin An, G. Zhou, W. Li, H. Wang, T. Duan, L. Jiang, and H. Yu, Electronics **7**, 377 (2018).
[6]J. Bergsten, J.-T. Chen, S. Gustafsson, A. Malmros, U. Forsberg, M. Thorsell, E. Janzen, and N. Rorsman, IEEE Trans. Electron Devices **63**, 333 (2016).
[7]K. Ahi, Opt. Eng. **56**, 090901 (2017).
[8]H. W. Hou, Z. Liu, J. H. Teng, T. Palacios, and S. J. Chua, Sci. Rep. **7**, 46664 (2017).
[9]H. Morkoc, *Handbook of Nitride Semiconductors and Devices* (Wiley-VCH, Weinheim, 2008), Vol. 1.
[10]J. P. Ibbetson, P. T. Fini, K. D. Ness, S. P. DenBaars, J. S. Speck, and U. K. Mishra, Appl. Phys. Lett. **77**, 250 (2000).
[11]V. N. Popok, T. S. Aunsborg, R. H. Godiksen, P. K. Kristensen, R. R. Juluri, P. Caban, and K. Pedersen, Rev. Adv. Mater. Sci. **57**, 72 (2018).
[12]S. W. Kaun, M. H. Wong, U. K. Mishra, and J. S. Speck, Appl. Phys. Lett. **100**, 262102 (2012).
[13]D. Christy, A. Watanabe, and T. Egawa, AIP Adv. **4**, 107104 (2014).
[14]M. J. Manfra, N. G. Weimann, J. W. P. Hsu, L. N. Pfeiffer, K. W. West, and S. N. G. Chu, Appl. Phys. Lett. **81**, 1456 (2002).
[15]S. Heikman, S. Keller, Y. Wu, J. S. Speck, S. P. DenBaars, and U. K. Mishra, J. Appl. Phys. **93**, 10114 (2003).
[16]I. Khalil, E. Bahat-Treidel, F. Schnieder, and J. Wurfl, IEEE Trans. Electron Devices **56**, 361 (2009).

[17]X. Wang, S. Huang, Y. Zheng, K. Wei, X. Chen, H. Zhang, and X. Liu, IEEE Trans. Elecron Devices **61**, 1341 (2014).
[18]A. Goyal, B. S. Yadav, R. Raman, and A. K. Kapoor, AIP Adv. **8**, 025021 (2018).
[19]S. Turuvekere, A. DasGupta, and N. DasGupta, IEEE Trans. Electron Devices **62**, 3449 (2015).
[20]Y. Takei, K. Tsutsui, W. Saito, K. Kakushima, H. Wakabayashi, and H. Iwai, Jpn. J. Appl. Phys. **55**, 040306 (2016).
[21]V. G. Tikhomirov, V. E. Zemlyakov, V. V. Volkov, Y. M. Parnes, V. N. Vyuginov, W. V. Lundin, A. V. Sakharov, E. E. Zavarin, A. F. Tsatsulnikov, N. A. Cherkashin, M. N. Mizerov, and V. M. Ustinov, Semiconductors **50**, 244 (2016).
[22]Y. Zhang, I. P. Smorchkova, C. R. Elsass, S. Keller, J. P. Ibbetson, S. Denbaars, U. K. Mishra, and J. Singh, J. Appl. Phys. **87**, 7981 (2000).
[23]R. Brown, D. Macfarlane, A. Al-Khalidi, X. Li, G. Ternent, H. Zhou, I. Thayne, and E. Wasige, IEEE Electron Device Lett. **35**, 906 (2014).
[24]V. N. Popok, A. Kalabukhov, R. Gunnarsson, S. Lemeshko, T. Claeson, and D. Winkler, J. Adv. Microsc. Res. **5**, 26 (2010).
[25]P. Gibart, Rep. Prog. Phys. **67**, 667 (2004).
[26]L. Zhang, K. H. Lee, I. M. Riko, C.-C. Huang, A. Kadir, K. E. Lee, S. J. Chua, and E. A. Fitzgerald, Semicond. Sci. Technol. **32**, 065001 (2017).
[27]S. P. Grabowski, M. Schneider, H. Nienhaus, W. Mönch, R. Dimitrov, O. Ambacher, and M. Stutzmann, Appl. Phys. Lett. **78**, 2503 (2001).
[28]M. S. Miao, J. R. Weber, and C. G. Van de Walle, J. Appl. Phys. **107**, 123713 (2010).
[29]A. S. Kalabukhov, Y. A. Boikov, I. T. Serenkov, V. I. Sakharov, V. N. Popok, R. Gunnarsson, J. Börjesson, N. Ljustina, E. Olsson, D. Winkler, and T. Claeson, Phys. Rev. Lett. **103**, 146101 (2009).
[30]M. P. Warusawithana, C. Richter, J. A. Mundy, P. Roy, J. Ludwig, S. Paetel, T. Heeg, A. A. Pawlicki, L. F. Kourkoutis, M. Zheng, M. Lee, B. Mulcahy, W. Zander, Y. Zhu, J. Schubert, J. N. Eckstein, D. A. Muller, C. Stephen Hellberg, J. Mannhart, and D. G. Schlom, Nat. Commun. **4**, 2351 (2013).